

Wide sensitive area of small foreshocks

Chieh-Hung Chen^{1,2*}, Yang-Yi Sun², Strong Wen³, Peng Han⁴, Li-Ching Lin⁵, Huai-Zhong Yu⁶, XueMin Zhang⁷, Yongxin Gao⁸, Chi-Chia Tang^{1,2}, Cheng-Horng Lin⁹, Jann-Yenq Liu^{10,11,12}

1. State Key Laboratory of Geological Processes and Mineral Resources, China University of Geosciences, Wuhan, China

2. Institute of Geophysics and Geomatics, China University of Geosciences, Wuhan, China

3. Department of Earth and Environmental Sciences, National Chung Cheng University, Chiayi, Taiwan

4. Department of Earth and Space Sciences, Southern University of Science and Technology, Shenzhen, China

5. **National Applied Research Laboratories**, Taipei, Taiwan

6. China Earthquake Networks Center, Beijing, China

7. Institute of Earthquake Forecasting, China Earthquake Administration, Beijing, China

8. School of Civil Engineering, Hefei University of Technology, Hefei, China

9. Institute of Earth Sciences, Academia Sinica, Taipei, Taiwan

10. **Graduate Institute of Space Science, National Central University, Taoyuan, Taiwan**

11. **Center for Space and Remote Sensing Research, National Central University, Taoyuan, Taiwan**

12. **Center for Astronautical Physics and Engineering, National Central University, Taoyuan, Taiwan**

*** Corresponding Author:**

Chieh-Hung Chen, E-mail: nononochchen@gmail.com

Institute of Geophysics and Geomatics,

30 China University of Geosciences, Wuhan, Hubei, 430074, China

31

32 **Abstract**

33 Scientists demystify stress changes within tens of days before a mainshock and
34 often utilize its foreshocks as an indicator. Typically, foreshocks are detected near
35 fault zones, which may be due to the distribution of seismometers. This study
36 investigates changes in seismicity far from mainshocks by examining tens of thousands
37 of $M \geq 2$ quakes that were monitored by dense seismic arrays for more than 10 years in
38 Taiwan and Japan. The quakes occurred within epicentral distances ranging from 0
39 km to 400 km during a period of 60 days before and after the mainshocks that are
40 utilized to exhibit common behaviors of seismicity in the spatiotemporal domain. The
41 superimposition results show that wide areas exhibit increased seismicity associated
42 with mainshocks being more than 50 times to areas of the fault rupture. The seismicity
43 increase initially concentrates in the fault zones, and gradually expands outward to over
44 50 km away from the epicenters approximately 40 days before the mainshocks. The
45 seismicity increases more rapidly around the fault zones approximately 20 days before
46 the mainshocks. The stressed crust triggers **ground vibrations** at frequencies varying
47 from $\sim 5 \times 10^{-4}$ Hz to $\sim 10^{-3}$ Hz (i.e., variable frequency) along with earthquake-related
48 stress that migrates from exterior areas to approach the fault zones. The variable
49 frequency is determined by the observation of continuous seismic waveforms through
50 the superimposition processes and is further supported by the resonant frequency model.
51 These results suggest that the variable frequency of ground vibrations is a function of
52 areas with increased seismicity leading to earthquakes.

53

54 Keywords: foreshocks; resonance frequency; earthquake-related stressed area

55

56 **1. Introduction**

57 Numerous studies (Reasenberg, 1999; Scholz, 2002; Vidale et al., 2001; Ellsworth
58 and Beroza, 1995) reported that foreshocks occur near a fault zone and migrate toward

59 the hypocenter of a mainshock before its occurrence. The spatiotemporal evolution
60 of foreshocks is generally considered to be an essential indicator that reveals variations
61 in earthquake-related stress a couple of days before mainshocks. After detecting these
62 variations, scientists installed multiple instruments along both sides of the fault over
63 short distances to monitor the activity of the fault. However, these instruments
64 typically detect small vibrations near the fault zone. Stress accumulates in a local
65 region near a hypocenter triggering earthquake occurrence that is concluded from the
66 sparse distribution of seismometers.

67 Bedford et al. (2020) analyzed the GNSS data and observed crustal deformation
68 in a thousand-kilometer-scale area before the great earthquakes in the subduction zones.
69 Chen et al. (2011, 2014, 2020a, 2020b) filtered the crustal displacements before
70 earthquakes using the GNSS data through the Hilbert-Huang transform. The filtered
71 crustal displacements in a hundred(thousand)-kilometer-scale area before the moderate-
72 large (M9 Tohoku-Oki) earthquakes exhibit paralleling azimuths that yield an
73 agreement with the most compressive axes of the forthcoming earthquakes. On the
74 other hand, Dobrovolsky (1979) estimated the size of the earthquake preparation zone
75 using the numerical simulation method and found that the radius (R) of the zone is
76 proportional to earthquake magnitude (M). In addition, the relationship can be written
77 by using a formula of $R=10^{0.43M}$. These results suggest that a stressed area before
78 earthquakes is obviously larger than the rupture of fault zones. However, it is a big
79 challenge to monitor stress changes in a wide area beneath the ground. A simple way
80 to imagine this is if we place a stick on a table, then hold and try to break the stick.
81 The stress we making on the stick can apply to either a limited local region or to both
82 ends of it. Migrations and propagations of the loading force can be detected according
83 to the changes of strain and the occurrence of microcracks. This common sense
84 suggests that the spatiotemporal evolution of earthquake-related stress appearing a
85 couple of days before mainshocks can be recognized if we can trace the occurrence of
86 relatively-small quakes in a wide area (Kawamura et al., 2014; Wen and Chen, 2017).
87 Here we take advantage of earthquake catalogs obtained by dense seismic arrays in

88 Taiwan and Japan to expose foreshocks distributing over a wide area instead of a local
89 region.

90

91 **2. Methodology**

92 The ability to detect relatively-small quakes depends on the spatial density and
93 capability of seismometers. Taiwan and Japan are both the most famous high-
94 seismicity areas in the world. Dense seismometers evenly distributed throughout the
95 whole area are beneficial for monitoring the earthquake occurrences near to and far
96 away from fault zones (Chang, 2014). Earthquake catalogs retrieved from Taiwan and
97 Japan were obtained from the Central Weather Bureau (CWB), Taiwan and the Japan
98 Meteorological Agency (JMA), respectively. To distinguish dependencies from
99 independent seismicity, the earthquake catalogs are declustered. Therefore, the
100 ZMAP software package for MATLAB (Weimer, 2001) was utilized to remove and/or
101 omit influence from duplicate events, such as aftershocks. The declustering algorithm
102 used in ZMAP is based on the algorithm developed by Reasenber (Reasenber, 1985).
103 We classify clusters by using the standard input parameters (proposed in Reasenber,
104 1985 and Uhrhammer, 1986) for the declustering algorithm. Because the aftershock
105 clusters in a small area and in a short period of time do not conform to the Poisson
106 distribution, which requires removing the aftershocks from the earthquake sequence.
107 Therefore, some parameters can be set as follow: The look-ahead time for un-clustered
108 events is in one day, and the maximum look-ahead time for clustered events is in 10
109 days. The measure of probability to detect the next event in the earthquake sequence
110 is 0.95. The effective minimum magnitude cut-off for the catalog is given by 1.5, and
111 the interaction radius of dependent events is given by 10 km (van Stiphout et al., 2012).
112 Earthquakes with depth > 30 km were eliminated from the declustered catalogs to
113 understand seismicity changes before mainshocks mainly in the crust.

114 Before the analytical processes in this study, we assumed that earthquakes with
115 relatively-small magnitude can be the cracks and potentially related to the far
116 mainshocks based on the large seismogenic areas (Bedford et al., 2020). The

117 minimum magnitudes of completeness M_c are 2.0 and 0.0 that can be determined by
118 the declustered earthquake catalogs in Taiwan and Japan, respectively (also see Figs.
119 S1–S4). The earthquakes with $M \geq 2$ are selected and utilized in this study for fair
120 comparison of the seismicity changes during earthquakes in Taiwan and Japan. We
121 classified the selected earthquakes via their magnitudes into three groups (i.e., $3 \leq M <$
122 4 , $4 \leq M < 5$ and $5 \leq M < 6$). Note that the classified earthquakes in each group are
123 determined as the break events (i.e., the mainshocks). In contrast, the other selected
124 earthquakes with magnitudes smaller than the minima of the classified magnitude are
125 determined as the crack events.

126 We construct a spatiotemporal distribution of the crack events for each break quake.
127 The spatiotemporal distribution from 0 km to 400 km away from the epicenter of the
128 break quake during a period of 60 days before and after the break occurrence is
129 constructed to illustrate the relationship between the crack events and the break quake
130 in the spatial and temporal domain. Note that the spatial and temporal resolutions of
131 the grids of the spatiotemporal distribution are 10 km and 1 day, respectively, based on
132 the declustering parameters in the ZMAP software (Weimer, 2001). We count the
133 crack events in each spatiotemporal grid according to distance away from the epicenter
134 and the differences in time before and after the occurrence of the break quake.

135 The superimposition process, a statistical tool utilized in data analysis, is capable
136 of either detecting periodicities within a time sequence or revealing a correlation
137 between more than two data sequences (Chree, 1913). The process is known as the
138 superposed epoch analysis (Adams et al., 2003; Hocke, 2008). In practice, the
139 superimposition is a process to stack numerous datasets that can migrate unique features
140 for a few datasets and enhance common characteristics for the most datasets. The
141 count in each grid of the spatiotemporal distributions for all the break quakes are
142 superimposed as a total one based on the occurrence time and epicentral distance of the
143 break quakes. The total count of the superimposed distribution in each spatiotemporal
144 grid is normalized to seismic density (count/km²) for comparing to the total number of
145 the break quakes and the related spatial area. Moreover, we compute the average

146 values every distance grid using the seismic densities 60 days before and after the quake.
147 The average values are subtracted from the seismic densities and the obtained
148 differences are divided by the average values in each distance grid to obtain the
149 normalized variation clarifying changes of the seismic density in the spatiotemporal
150 domain.

151

152 3. Analytical results

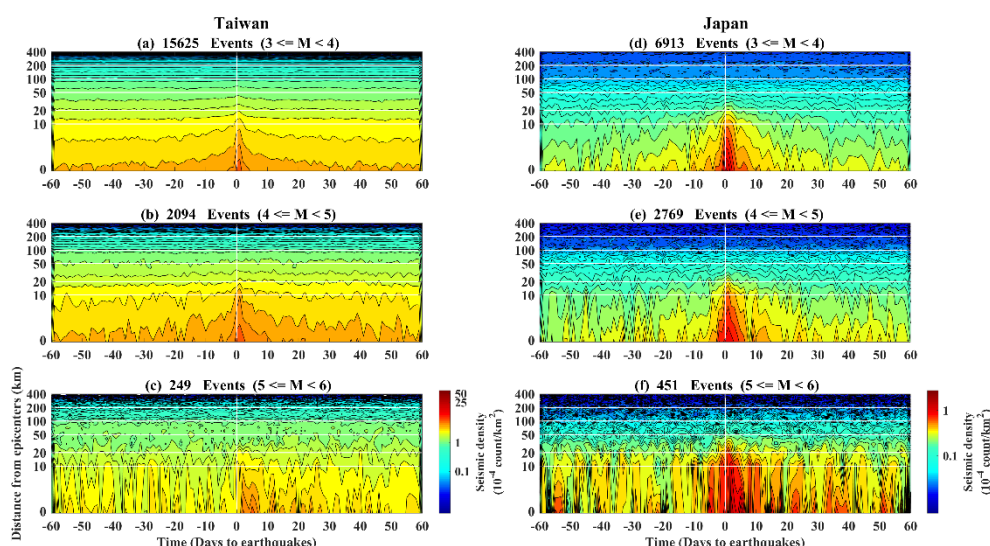
153 The earthquakes with magnitude ≥ 2 listed in the declustered catalogs of Taiwan
154 from January 1991 to June 2017 are utilized to construct a spatiotemporal distribution
155 of foreshocks and aftershocks corresponding to the quakes with $3 \leq M < 4$. We
156 superimposed all the crack events corresponding to the 15625 quakes ($3 \leq M < 4$).
157 The seismic density is more than 1000 times greater in a hot region at a distance of 10
158 km away from an epicenter (which is generally considered to be the gestation area of
159 foreshocks) than it is in areas located > 200 km from the epicenter (Fig. 1a). The
160 sudden increase of seismic density suggests that earthquake-related stress accumulates
161 mainly around the hot region, triggering many foreshocks a few days before the
162 earthquakes with $3 \leq M < 4$. This partial agreement of the numerous recent studies
163 reported that the seismicity migrates toward the fault rupture zone within tens of
164 kilometers from epicenters a couple of days before earthquakes (Kato et al., 2012, Kato
165 and Obara, 2014; Liu et al., 2019). Meanwhile, the events mainly occur 0–1 day after
166 the quakes that is irrelevant to the smaller distribution 0–1 day before the quakes (also
167 see Fig. 1). The seismic density close to epicenters (Fig. 1) suddenly increases before
168 and gradually decreases after the quakes. The irrelevance and the differences of
169 changes rates with epicentral distance smaller than 20 km before and after the quakes
170 reveal that the increase of seismicity before the quakes is not contributed by the
171 seismicity after due to the analytical processes in this study. In addition, these
172 analytical results of the seismic activity are also in agreement with the studies in
173 Lippiello et al. (2012, 2017, 2019) and de Arcangelis et al. (2016) regard for distinct
174 methods.

175 On the other hand, the increase of seismic density is not only always limited within
176 the hot region, but also extends outward to a distance of over 50 km away from the
177 epicenters about 0–40 days leading up to the occurrence of the quakes (Fig. 1a). We
178 further examine the spatiotemporal changes in the seismic density up to the $M \geq 4$
179 quakes utilizing the same superimposition process (Figs. 1b–c). The expansion of the
180 increased seismic density about 0–40 days leading up to the occurrence of the quakes
181 and the sharp increases of seismic density a few days before the quakes that can be
182 consistently observed using the $M \geq 4$ quakes in Figs. 1b–c. **Similar results (i.e., the**
183 **sharp increases of seismic density a few days before the quakes and areas where the**
184 **increase of the seismicity density is much larger than that of the hot region) can also be**
185 **obtained using the earthquake catalogs between 2001 and 2010 from the Japan**
186 **Meteorological Agency (JMA) in Japan (Figs. 1d–f). Note that the earthquakes that**
187 **occurred in the northern side of the latitude of 32°N were selected from the Japan**
188 **catalogs. The selection is based on that the earthquakes occurred in the area monitored**
189 **by the dense seismometer network and to avoid the double count of events in the**
190 **Taiwan catalogs.** The normalized variations correspond to seismic density in Fig. 1
191 are shown in Fig. 2. The radii of the positive normalized variations are approximately
192 50 km while earthquake magnitude increases from 3 to 6 in Taiwan (Figs. 2a–c). The
193 land area of Taiwan is approximately 250 km by 400 km, which causes underestimation
194 of the seismic density in the spatial domain. In contrast, the positive normalized
195 variations roughly expand along the radii ranging from 50 km to 150 km, while
196 earthquake magnitude increases from 3 to 6 in Japan (Figs. 2d–f). However,
197 variations in the lead time mostly range from 40 days to 20 days, and relationships
198 between the positive normalized variations and the earthquake magnitude can be found
199 neither in Taiwan nor Japan (Fig. 2).

200 **In short, the expansion of the increase of seismic density becomes mitigation and**
201 **may no longer be impact a place at distances > 200 km away from the epicenters for**
202 **the earthquakes with magnitude < 6 .** The increase of seismicity density before the
203 quakes suggests that the accumulation of the earthquake-related stress in the crust

204 originates from the hot region, and gradually extends to an external place before
 205 earthquakes occur. The area of this external place is several times that of a fault
 206 rupture zone that is concluded based on the sparse seismic arrays of the past. If a
 207 quake can excite seismicity changes over a wide area (i.e., over 50 km by 50 km), any
 208 crustal vibration related to stress accumulation before earthquakes can be too small to
 209 be identified from continuous seismic waveforms at one station. In contrast, crustal
 210 vibrations can be a common characteristic of continuous seismic waveforms at most
 211 stations around fault zones due to that seismicity changes dominated by earthquake-
 212 related stress accumulation distributes in a wide area.

213

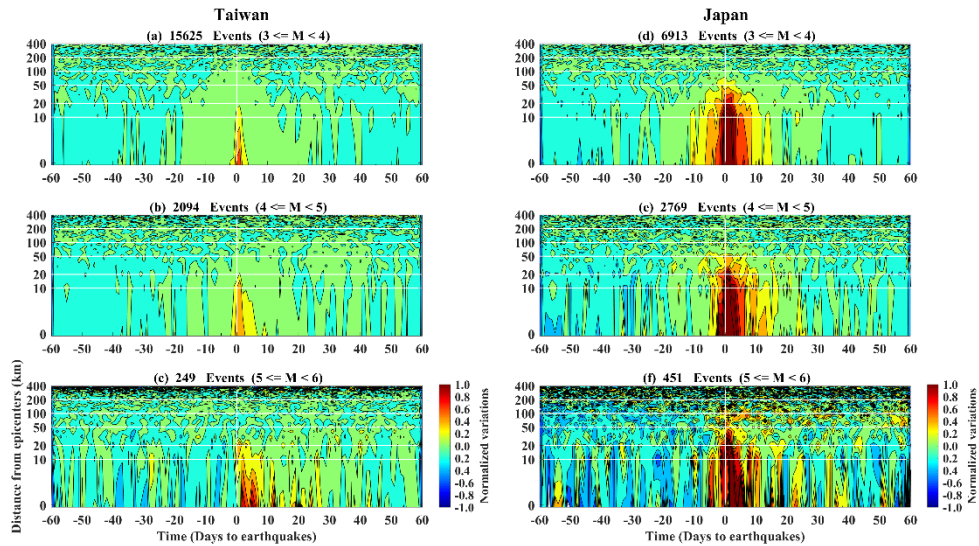


214

215

216 Fig. 1. Spatiotemporal seismic density distributions in Taiwan and Japan. The
 217 seismic densities constructed by using the declustered earthquake catalogs of Taiwan
 218 and Japan are shown in the left and right panels, respectively. The seismic density
 219 reveals changes in seismicity at distances from the epicenters ranging from 0 km to 400
 220 km at up to 60 days before and after quakes in a particular magnitude group. The
 221 superimposed number in each grid is further normalized for a fair comparison by using
 222 the total number of quakes and their areas. Notably, the total number of quakes is
 223 shown in the title of each diagram.

224



225

226

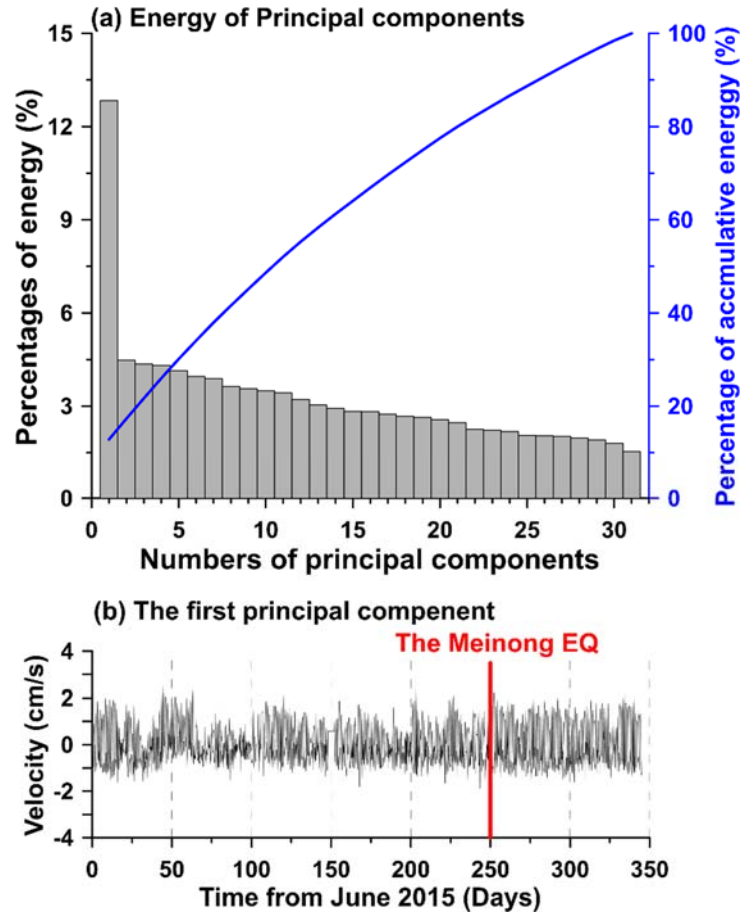
227 Fig. 2. Changes of the normalized spatiotemporal variations in Taiwan and Japan.
 228 The normalized variations correspond to the seismic density in Taiwan and Japan (in
 229 Fig. 1) are shown in the left and right panels, respectively. The colors reveal changes
 230 of the normalized variations at distances from the epicenters ranging from 0 km to 400
 231 km at up to 60 days before and after quakes in a particular magnitude group.

232

233 4. The principal component analysis (PCA) on the continuous seismic waveforms

234 Seismic waveforms obtained from 33 broadband seismometers operated by
 235 National Center for Research on Earthquake Engineering (NCREE) of Taiwan, within
 236 a temporal span of approximately one year (from June 2015 to June 2016) are utilized
 237 in this study. Note that two seismometers of them are eliminated from following the
 238 analytical processes due to long data gaps. The principal component analysis (PCA)
 239 method (Jolliffe, 2002) is utilized to retrieve the possible stress-related common signals
 240 from continuous seismic waveforms on the vertical component at thirty-one seismic
 241 stations over a wide area and to mitigate local noise simultaneously. Fig. 3a shows
 242 that the energy and the cumulative energy of the principal components derived from the
 243 continuous seismic waveforms at the 31 stations. The energy of the first principal
 244 component is about 12% that is more than 3 times to the following ones. Thus, we
 245 determined the first principal component to be the common signals of the ground

246 vibrations before earthquakes. Fig. 3b reveals changes in the common signals during
 247 the study period along the time. However, no obvious changes can be observed in the
 248 temporal domain.
 249

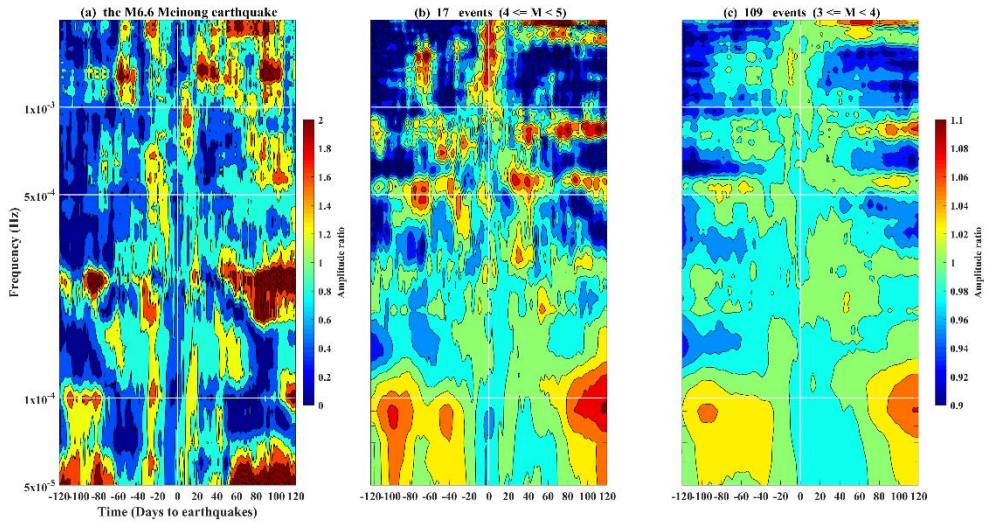


250
 251 Fig. 3. The energy and the first principal component derived from vertical seismic
 252 velocity data from the 31 stations. The energy and the cumulative energy of the
 253 principal components are shown in (a). Bars denote the energy of each principal
 254 component. The blue line shows the variation of the cumulative energy from distinct
 255 used principal components. The variations of the first principal component during the
 256 period (i.e., from June 2015 to June 2016) are revealed in (b). The red vertical line
 257 indicates the occurrence time of the M6.6 Meinong earthquake (on February 2, 2016).

258 Thus, we sliced the common signals into several time spans using a 5-day moving
 259 window with one-day steps to show time-varying changes. The common signals in
 260 each time span are transferred into the frequency domain using the Fourier transform
 261 to investigate frequency characteristics of ground vibrations before earthquakes. The

262 amplitudes are normalized using the frequency-dependent average values computed
263 from the amplitude 30 days before and after earthquakes via the temporal division.
264 Here, we take the M6.6 Meinong earthquake (Wen and Chen, 2017) as an example to
265 understand the changes of the amplitude of the common signals in the spatiotemporal
266 domain (Fig. 4a). Distinct patterns in the amplitude-frequency distributions can
267 obviously be observed before and after the earthquake at frequency close to 5×10^{-4} Hz.
268 The amplitude at the frequency close to 5×10^{-4} Hz was obviously enhanced
269 approximately 20–40 days before the earthquake. Hereafter, the enhancements were
270 significantly reduced and reached to a relatively-small value a few days after the
271 earthquake. Meanwhile, the frequency is close to 5×10^{-4} Hz approximately 60 days
272 before the earthquake and tends to be high near 10^{-3} Hz a few days before the event.

273 We next superimpose the amplitude based on the occurrence time of the 17
274 earthquakes with $4 \leq M < 5$ and the 109 earthquakes with $3 \leq M < 4$ during the one-
275 year temporal span shown in Figs. 4b and 4c, respectively. The consistent variations
276 (i.e., the frequency is close to 5×10^{-4} Hz approximately some days before the quakes
277 tending to be high near 10^{-3} Hz a few days before the quakes) that can be observed in
278 Figs. 4b and 4c. Note that the amplitudes of the variable frequency patterns are
279 proportional to the earthquake magnitude. These results suggest that the common-
280 mode ground vibrations exist in a wide area before earthquakes due to the signals being
281 retrieved from the most stations distributing the whole Taiwan island through the PCA
282 method. In short, the common-mode vibrations are very difficult to be identified from
283 the time-series data but become significant in the frequency domain. If the expansion
284 of the seismoenergetic areas and the existence of the common-mode ground vibrations are
285 true, the next step is to determine the potential mechanism hidden behind this nature.



286

287 Fig. 4. The amplitude ratio of the superimposed time-frequency-amplitude distribution
 288 associated with earthquakes with distinct magnitudes. The superimposed results
 289 related to quakes with the M6.6 Meinong earthquake, $4 \leq M < 5$ and $3 \leq M < 4$
 290 are shown in (a), (b) and (c), respectively. The distribution is normalized for comparison
 291 by using the average amplitude in each particular frequency band of 30 days before and
 292 after the quakes. The total number of earthquakes in each magnitude group is shown
 293 in the title of each diagram.

294

295 5. Discussions

296 Walczak et al. (2017) repeatedly observed stressed rocks exciting long-period
 297 vibrations during rock mechanics experiments. Leissa (1969) reported that the
 298 resonance frequency of an object is proportional to its Young's modulus and exhibits
 299 an inverse relationship to its mass. Based on the crust, the outermost of the Earth, is
 300 lamellar, we assume that the earthquake-related stress accumulates in the volume of a
 301 square sheet with a width of 100 km, which is determined by using a distance of 50 km
 302 away from an earthquake due to the significant increase of the seismic density (Figs. 1
 303 and 2). The resonance frequency near 3×10^{-4} Hz (Fig. 4) can be derived from the
 304 square sheet once the thickness of the volume is ranged between 500 meters and 1000
 305 meters (Fig. S5). Although we do not fully understand the causal mechanism of the
 306 thickness, the agreement with the spatiotemporal domain of the relatively-small quakes

307 from the earthquake catalogs, the superimposition results of continuous seismic
308 waveforms and the resonance frequency models suggest that the phenomenon of
309 variable frequency may exist tens of days before earthquake occurrence and can be
310 retrieved by broadband seismometers.

311 In this study, we determined the seismogenic areas using the relatively-small
312 earthquakes in the spatiotemporal distribution and found that the areas are significantly
313 larger than the fault rupture zone (Figs. 1 and 2). Meanwhile, the ground vibrations
314 can exhibit frequency-dependent characteristics at about 10^{-4} Hz (Fig. 4) that could
315 relate to the large seismogenic areas due to the resonance model (Fig. S5). If these
316 are true, the seismo-TEC (total electron content) anomalies in the ionosphere, which is
317 generally observed in a large-scale area with more than ten thousand square kilometers
318 (Liu et al., 2009), are high potential to be driven by upward propagation of acoustic
319 waves before earthquakes (Molchanov et al., 1998, 2011; Korepanov et al., 2009;
320 Hayakawa et al., 2010, 2011; Sun et al., 2011; Oyama et al., 2016). The existence of
321 the ground vibrations can generate the acoustic-gravity waves that have been reported
322 (Liu et al., 2016, 2017). However, the acoustic-gravity waves in a period of < 300
323 seconds are difficult to propagate upward into the atmosphere and the ionosphere (Yeh
324 and Liu, 1974; Azeem et al., 2018). The wide seismogenic areas observed in this
325 study can contribute the larger-scale ground vibrations at approximately $5 \times 10^{-4} - 10^{-3}$
326 Hz that cover the frequency channel ($< 1/300$ Hz) for the acoustic-gravity waves
327 propagating into the atmosphere and changing the TEC in the ionosphere. Meanwhile,
328 the seismo-atmospheric and the seismo-ionospheric anomalies in a large-scale area can
329 also be supported by the acoustic-gravity waves due to the wide seismogenic areas.
330 While partial aforementioned relationships cannot be quickly proven, the ground
331 vibrations at a low frequency ($< 1/300$ Hz) in a wide area assist our understanding of
332 the essence of the seismo-anomalies in the atmosphere and the ionosphere.

333

334 **6. Conclusion**

335 The process of stress migration in the spatiotemporal domain can be concluded

336 from tracing the increase of seismicity according to the 10-year earthquake catalogs
337 from dense seismic arrays in Taiwan and Japan. Areas with the increase of seismicity,
338 where stress accumulates in the crust triggering earthquakes are serious
339 underestimation using a sparse seismic array. Seismicity initially increases around
340 hypocenters, and this can be observed more than 50 days before quakes through
341 superimposing large numbers of earthquakes. The seismicity gradually increases
342 along with the expansion of areas from fault zones to an area widely covering an
343 epicentral distance close to 50 km approximately 20–40 days before earthquakes. The
344 crustal resonance exists at a frequency near 5×10^{-4} Hz when the expansion becomes
345 insignificant. Instead of the spatial expansion, the sharp increase of seismicity around
346 the hot regions suggests stress accumulation in fault zones generating crustal resonance
347 at a frequency of up to $\sim 10^{-3}$ Hz in the few days before earthquakes. Most broadband
348 seismometers can observe the variable frequency of ground vibrations in Taiwan due to
349 the comprehensive spatial coverage of resonant signals. The variable frequency
350 depends on various stress-dominant areas that can be supported by the potential crustal
351 resonance model. Seismic arrays comprise dense seismometers with a wide coverage
352 are beneficial for monitoring the comprehensive process of stress migration in the
353 spatiotemporal domain leading up to a faraway and forthcoming mainshock.

354

355 **Acknowledgements.** The authors appreciate scientists who devote to maintain
356 instruments in the field and data centers in the office that leads chances to expose such
357 interesting geophysical phenomena and understand potential processes during
358 seismogenic periods. This research was funded by National Key R&D Program of
359 China, grant number 2018YFC1503705; National Natural Science Foundation of China
360 (Grants No. 41474038 and 41774048); the Spark Program of Earthquake Science of
361 China (Grant No. xh17045); Ministry of Science and Technology of Taiwan (Grants
362 No. MOST 106-2116-M-194-016- and MOST 106-2628-M-008-002), and Sichuan
363 earthquake Agency-Research Team of GNSS based geodetic tectonophysics and
364 mantle-crust dynamics of Chuan-Dian region (Grant No. 201803). Meanwhile, this

365 work was also supported by the Center for Astronautical Physics and Engineering
366 (CAPE) from the Featured Area Research Center program within the framework of
367 Higher Education Sprout Project by the Ministry of Education (MOE) in Taiwan.

368

369 **References**

- 370 Adams, J.B., Mann, M.E., and Ammann, C.M.: Proxy evidence for an El Niño-like
371 response to volcanic forcing, *Nature*, 426, 274–278, 2003.
- 372 Azeem, I., Walterscheid, R. L. and Crowley, G.: Investigation of acoustic waves in the
373 ionosphere generated by a deep convection system using distributed networks of
374 GPS receivers and numerical modeling, *Geophys. Res. Lett.*, 45, 8014–8021,
375 2018.
- 376 Bedford, J.R., Moreno, M., Deng, Z. et al.: Months-long thousand-kilometre-scale
377 wobbling before great subduction earthquakes, *Nature*, 580, 628–635, 2020.
- 378 Chang, C.H.: Introduction to the Meteorological Bureau Earthquake Monitoring
379 Network, Taiwan Earthquake Research Center Newsletter, 2014.
- 380 Chen, C.-H., Yeh, T.-K., Wen, S., Meng, G., Han, P., Tang, C.-C., Liu, J.-Y. and Wang,
381 C.-H.: Unique Pre-Earthquake Deformation Patterns in the Spatial Domains from
382 GPS in Taiwan, *Remote Sens.*, 12, 366, 2020a.
- 383 Chen, C.-H., Su, X., Cheng, K.-C., Meng, G., Wen, S., Han, P., Tang, C.-C., Liu, J.-Y.
384 and Wang, C.-H.: Seismo-deformation anomalies associated with the M6.1
385 Ludian earthquake on August 3, 2014, *Remote Sens.*, 12, 1067, 2020b.
- 386 Chen, C.H., Wen, S., Liu, J.Y., Hattori, K., Han, P., Hobara, Y., Wang, C.H., Yeh, T.K.
387 and Yen, H.Y.: Surface displacements in Japan before the 11 March 2011 M9.0
388 Tohoku-Oki earthquake, *J. Asian Earth Sci.*, 80, 165–171, 2014.
- 389 Chen, C.H., Yeh, T.K., Liu, J.Y., Wang, C.H., Wen, S., Yen, H.Y. and Chang, S.H.:
390 Surface Deformation and Seismic Rebound: implications and applications, *Surv.*
391 *Geophys.*, 32(3), 291–313, 2011.
- 392 Chree, C.: Some phenomena of sunspots and of terrestrial magnetism at Kew
393 observatory, *Phil. Trans. R. Soc.*, 212, 75, 1913.

394 de Arcangelis, L., Godano, C., Grasso, J.R. and Lippiello, E.: Statistical physics
395 approach to earthquake occurrence and forecasting, *Phys. Rep.*, 628, 1–91, 2016.

396 Dobrovolsky, I.P., Zubkov, S.I. and Miachkin, V.I.: Estimation of the size of earthquake
397 preparation zones, *Pure Appl. Geophys.*, 117, 1025–1044, 1979.

398 Ellsworth, W.L., and Beroza, G.C.: Seismic evidence for an earthquake nucleation
399 phase, *Science*, 268, 851–855, 1995.

400 Hayakawa, M., Kasahara, Y., Nakamura, T., Hobara, Y., Rozhnoi, A., Solovieva, M.,
401 Molchanov, O. and Korepanov, V.: Atmospheric gravity waves as a possible
402 candidate for seismo-ionospheric perturbations, *J.Atmos. Electr.*, 31, 129–140,
403 2011.

404 Hayakawa, M., Kasahara, Y., Nakamura, T., Muto, F., Horie, T., Maekawa, S., Hobara,
405 Y., Rozhnoi, A.A., Solovieva, M. and Molchanov, O.A.: A statistical study on the
406 correlation between lower ionospheric perturbations as seen by subionospheric
407 VLF/LF propagation and earthquakes, *J. Geophys. Res.*, 115, A09305, 2010,

408 Hocke, K., Oscillations of global mean TEC, *J. Geophys. Res.*, 113, A04302,
409 <https://doi.org/10.1029/2007JA012798>, 2008.

410 Jolliffe, I.T.: *Principal Component Analysis*, second edition, Springer, 2002.

411 Kato, A., and Obara, K.: Step-like migration of early aftershocks following the 2007
412 Mw 6.7 Noto-Hanto earthquake, Japan, *Geophys. Res. Lett.*, 41, 3864–3689,
413 <https://doi.org/10.1002/2014GL060427>, 2014.

414 Kato, A., Obara, K., Igarashi, T., Tsuruoka, H., Nakagawa, S., and Hirata, N.:
415 Propagation of slow slip leading up to the 2011 Mw9.0 Tohoku-Oki earthquake,
416 *Science*, 335, 705–708, <https://doi.org/10.1126/science.1215141>, 2012.

417 Kawamura, M., Chen, C.C., and Wu, Y.M.: Seismicity change revealed by ETAS, PI,
418 Z-value methods: A case study of the 2013 Nantou, Taiwan earthquake,
419 *Tectonophysics*, 634, 139–155, 2014.

420 Korepanov, V., Hayakawa, M., Yampolski, Y., Lizunov, G.: AGW as a seismo-
421 ionospheric coupling responsible agent, *Phys. Chem. Earth*, 34, 485–495, 2009.

422 Leissa, A.W., *Vibrations of plates*. Ohio State University, Columbus, Ohio, 1969.

423 Lippiello, E., Giacco, F., Marzocchi, W., Godano, C. and Arcangelis, L.D.: Statistical
424 Features of Foreshocks in Instrumental and ETAS Catalogs, *Pure Appl. Geophys.*,
425 174, 1679–1697, 2017.

426 Lippiello, E., Godano, C. and de Arcangelis, L.: The Relevance of Foreshocks in
427 Earthquake Triggering: A Statistical Study, *Entropy*, 21, 173, 2019.

428 Lippiello, E., Marzocchi, W., de Arcangelis, L. and Godano, C.: Spatial organization
429 of foreshocks as a tool to forecast large earthquakes, *Sci. Rep.*, 2, 846, 2012.

430 Liu, J.Y., Chen, C.H., Sun, Y.Y., Chen, C.H., Tsai, H.F., Yen, H.Y., Chum, J., Lastovicka,
431 J., Yang, Q.S., Chen, W.S. and Wen, S.: The vertical propagation of disturbances
432 triggered by seismic waves of the 11 March 2011 M9.0 Tohoku Earthquake over
433 Taiwan, *Geophys. Res. Lett.*, 43, 1759–1765, 2016.

434 Liu, J.Y., Chen, C.H., Wu, T.Y., Chen, H.C., Hattori, K., Bleier, T., Kappler, K., Yang,
435 I.C., Xia, Y., Chen, W. and Liu, Z.: Co-seismic signatures in magnetometer,
436 geophone, and infrasound data during the Meinong Earthquake, *Terr. Atmos.*
437 *Ocean Sci.*, 28(5), 683–692, 2017.

438 Liu, J.Y., et al.: seismoionospheric GPS total electron content anomalies observed
439 before the 12 May 2008 Mw 7.9 Wenchuan earthquake, *J. Geophys. Res.*, 114,
440 A04320, 2009.

441 Liu, S., Tang, C.C., Chen, C.H., and Xn, R.: Spatiotemporal Evolution of the 2018
442 Mw 6.4 Hualien Earthquake Sequence in Eastern Taiwan, *Seismol. Res. Lett.*,
443 <https://doi.org/10.1785/0220180389>, 2019.

444 Molchanov, O.A., and Hayakawa, M.: Subionospheric VLF signal perturbations
445 possibly related to earthquakes, *J. Geophys. Res. Space Phys.*, 103, 17489–17504,
446 1998.

447 Molchanov, O.A., Hayakawa, M. and Miyaki, K.: VLF/LF sounding of the lower
448 ionosphere to study the role of atmospheric oscillations in the lithosphere-
449 ionosphere coupling, *Adv. Polar Up. Atmos. Res.*, 15, 146–158, 2011.

450 Oyama, K.-I., Devi, M., Ryu, K., Chen, C.-H., Liu J.-Y., Liu, H., Bankov, L. and

451 Kodama, T.: Modifications of the ionosphere prior to large earthquakes: report
452 from the Ionosphere Precursor Study Group, *GeoSci. Lett.*, 3–6, 2016.

453 Reasenberg, P.: Second-order moment of central California seismicity, 1969-82, *J.*
454 *Geophys. Res.*, 90, 5479–5495, 1985.

455 Reasenberg, Paul A.: Foreshock occurrence before large earthquakes, *J. Geophys. Res.*,
456 104, 4755–4768, 1999.

457 Scholz, C.H.: *The Mechanics of Earthquakes and Faulting*. second edition, Cambridge
458 University Press, Cambridge, UK, 2002.

459 Sun, Y.Y., Oyama, K.-I., Liu, J.Y., Jhuang, H.K. and Cheng, C.Z.: The neutral
460 temperature in the ionospheric dynamo region and the ionospheric F region
461 density during Wenchuan and Pingtung Doublet earthquakes, *Nat. Hazards Earth*
462 *Syst. Sci.*, 11, 1759–1768, 2011.

463 Uhrhammer, R.: Characteristics of northern and southern California seismicity:
464 *Earthquake Notes*, 57, 21, 1986.

465 van Stiphout, T., Zhuang, J. and Marsan, D.: Seismicity declustering, *Community*
466 *Online Resource for Statistical Seismicity Analysis*, 2012,
467 doi:10.5078/corssa52382934. Available at <http://www.corssa.org>.

468 Vidale, J., Mori, J., and Houston, H.: Something wicked this way comes: Clues from
469 foreshocks and earthquake nucleation, *Eos Trans. AGU*, 82, 68, 2001.

470 Walczak, P. et al.: Real time observation of granular rock analogue material
471 deformation and failure using nonlinear laser interferometry, arXiv preprint,
472 arXiv:1705.03377v1, 2017.

473 Wen, Y.-Y., and Chen, C.-C.: Seismicity variations prior to the 2016 ML 6.6 Meinong,
474 Taiwan earthquake, *Terr. Atmos. Ocean. Sci.*, 28, 739–744,
475 <https://doi.org/10.3319/TAO.2016.12.05.01>, 2017.

476 Wiemer, S.: A Software Package to Analyze Seismicity: ZMAP, *Seismol. Res. Lett.*,
477 72, 373–382, <https://doi.org/10.1785/gssrl.72.3.373>, 2001.

478 Yeh, K.C. and Liu, C.H.: Acoustic-gravity waves in the upper atmosphere, *Rev.*

479 Geophys., 12(2), 193– 212, 1974.

480

481 **Data available**

482 The earthquake catalogs of Taiwan and Japan were obtained from the Central Weather
483 Bureau (<https://www.cwb.gov.tw/>), and the Japan Meteorological Agency (JMA;
484 <https://www.jma.go.jp/jma/indexe.html>), respectively. Seismic waveform data in
485 Taiwan were provided by the Seismic Array of NCREE in Taiwan (SANTA;
486 <https://www.ncree.narl.org.tw/>; please find the bottom for the English version in the top
487 right side). The downsampled seismic waveforms with the temporal interval of 10
488 seconds can be utilized to reproduce the analytical results in this study through the
489 MATLAB software that can be download at
490 <https://doi.org/10.5061/dryad.1jwstqjqq>.

491

492 **Author contribution**

493 Y.Y.S. contributed discussion and revision; S.W. contributed discussion and revision;
494 P.H. contributed data collection; L.C.L. contributed discussion and revision; H.Z.Y.
495 contributed discussion; X.Z. contributed discussion; Y.G. contributed discussion; C.C.T.
496 contributed discussion and revision; C.H.L. contributed discussion and revision; J.Y.L.
497 contributed discussion and revision.

498

499 **Competing interests**

500 The authors declare that they have no known competing financial interests or personal
501 relationships that could have appeared to influence the work reported in this paper.

502